Deposition Properties of Biomass Fly Ash

Laxminarayan, Yashasvi; Jensen, Peter Arendt; Wang, Guoliang; Wu, Hao; Sander, B.; Jappe Frandsen, Flemming; Glarborg, Peter

Published in:
Proceedings of 26th European Biomass Conference and Exhibition

Link to article, DOI:
10.5071/26thEUBCE2018-2AO.8.2

Publication date:
2018

Document Version
Peer reviewed version

DEPOSITION PROPERTIES OF BIOMASS FLY ASH

Y. Laxminarayan[1*], P.A. Jensen[1], G. Wang[1], H. Wu[1], B. Sander[2], F.J. Frandsen[1], P. Glarborg[1]
[1] Department of Chemical and Biochemical Engineering, Technical University of Denmark
Søltofts Plads 229, 2800 Kgs. Lyngby, Denmark
[2] Ørsted Bioenergy & Thermal Power A/S, Kraftsværksvej 53, Skærbæk, DK-7000, Fredericia, Denmark
*Corresponding author: ylax@kt.dtu.dk

ABSTRACT: This study investigated deposit formation of biomass fly ash on steel tubes, in a lab-scale Entrained Flow Reactor. Experiments were conducted using model biomass fly ash, prepared from mixtures of $K_2Si_4O_9$, KCl, K_2SO_4, CaO, SiO_2 and KOH, as well as three different boiler fly ashes: a wood fly ash, a straw fly ash, and a straw + wood cofired fly ash. The fly ashes were injected into the reactor, to form deposits on an air-cooled deposit probe, simulating deposit formation on superheater tubes in boilers. The results revealed that increasing flue gas temperature, probe surface temperature, time, fly ash flux and fly ash particle size increased the rate of deposit formation. However, increasing flue gas velocity resulted in a decrease in the deposit formation rate. A mechanistic model was developed for predicting deposit formation in the reactor. Inertial impaction was the primary mechanism of deposit formation, when pure $K_2Si_4O_9$, SiO_2 or CaO was injected into the reactor, forming deposits only on the upstream side of the steel tube. However, feeding KCl, K_2SO_4 or KOH into the reactor resulted in deposit formation on both sides of the steel tube, via condensation, thermophoresis, and inertial impaction.

Keywords: biomass, fly ash, deposit formation, fouling, ash sticking probability, entrained flow reactor

1 INTRODUCTION

Combustion of biomass for electricity and heat production is a promising solution for reducing net CO_2 emissions. Denmark is planning to phase out coal by 2030, with intentions to replace coal with biomass in pulverized fuel-fired power plants [1]. However, the inorganic content in biomass causes several operational problems, including increased deposition of chemically aggressive ash species (such as KCl and KOH) on boiler surfaces. Ash deposits hinder heat transfer to steam cycle, thereby reducing boiler efficiency, and may completely block flue gas channels in severe cases, causing unscheduled boiler shut-downs [2,3]. Moreover, ash deposition may cause severe corrosion of boiler surfaces [4]. Therefore, reducing deposit formation is essential for maximizing boiler efficiency and availability.

During combustion, the inorganic content in solid fuels undergoes several chemical and physical transformations. The volatile compounds are released into the gas phase, whereas the non-volatile residual ash particles may be entrained into the flue gas channel, forming fly ash [3,5]. Since the flue gas cools down as it flows through the boiler, it may become supersaturated with vapor species, resulting in either homogeneous condensation of vapors, forming submicron aerosol particles, or heterogeneous condensation of vapors on fly ash particles [3,6]. The formation of aerosols is typically initiated by homogeneous condensation of K_2SO_4, followed by coagulation and heterogeneous condensation of K_2SO_4 and KCl [7,8]. Therefore, the inorganic content in the flue gas may exist as vapor species, submicron aerosol particles, and larger (>10 µm) fly ash particles, which may subsequently form deposits on boiler surfaces.

The vapor species may undergo diffusion and heterogeneous condensation on heat transfer surfaces through the thermal boundary layer. Deposition of submicron aerosol particles may occur via thermophoresis, Brownian motion or eddy diffusion [9–11]. Thermophoresis occurs when the ash particles experience collisions from the hot flue gas molecules with a greater kinetic energy, when compared to cold flue gas molecules, thereby inducing a net force and movement of particles towards the cold heat transfer surface. Furthermore, vapors in the flue gas may undergo homogeneous condensation in the thermal boundary layer, forming aerosol particles, which may undergo thermophoretic deposition [10].

Deposition of larger fly ash particles primarily occurs via inertial impaction, which is dependent on the concentration of fly ash in the flue gas (fly ash flux), the flue gas and fly ash particle velocities, the impaction efficiency and the sticking probability of the fly ash particles to the boiler surface [11]. While detailed impaction efficiency models describing the flow of entrained particles around an obstacle exist in literature [12,13], quantification of the sticking probability has been a challenge. Simple sticking models correlate the sticking probability, $\eta(T)$, with the viscosity of the particles and the surface of the deposit, where decreasing particle/deposit surface viscosity results in an increased sticking probability, as shown below [14],

$$\eta(T) = \begin{cases} \frac{\mu_{ref}}{\mu} & \mu > \mu_{ref} \\ 1 & \mu \leq \mu_{ref} \end{cases} \quad (1)$$

where µ is the viscosity of the particle/deposit surface, and μ_{ref} is a reference viscosity, such that particles (or deposit surface) with viscosities lower than the reference viscosity are perfectly sticky. The net mass fraction of the impacting particles undergoing deposition, f_{dep}, is a function of the sticking probability of the ash particles, and the deposit surface, as shown below [11,14],

$$f_{dep} = p(T_g) + p(T_s)[1 - p(T_g)] \quad (2)$$

where T_g and T_s are the gas and deposit surface temperatures, and the gas temperature is assumed to be equal to the particle temperature.

Viscosity based models are unable to accurately predict the sticking probability when the ash composition is dominated by alkali salts. Alkali salts may form a melt and alter the ash sticking behavior [9]. In such cases, the sticking probability may be empirically expressed as a

function of the melt fraction of the particle/deposit surface (f_{melt}), where the sticking probability increases with increasing melt fraction, as shown below, [11]

$$\eta(T) = \begin{cases} 0 & 0 \le f_{melt} < 0.1 \\ 1.67 \cdot f_{melt} - 0.167 & 0.1 < f_{melt} < 0.7 \\ 1 & 0.7 < f_{melt} \le 1 \end{cases} \quad (3)$$

In the low temperature region of the boilers, where the ash predominantly exists as solid particles, deposition can be described using detailed models incorporating the viscoelastic behavior of ash particles, the particle size and velocity [9,15–17]. When viscoelastic particles collide with the deposit, they deform and dissipate energy. If the kinetic energy of the impacting particles is greater than the energy dissipated, the particles rebound from the deposit surface [18]. Such models define a critical velocity of the incoming particle $(u_{p,crit})$ as a function of the diameter (d_p), density (ρ_p), interface energy (surface tension) (Γ) and Young's modulus (E) of the particles, such that deposition occurs if the particle velocity is lower than the critical velocity.

$$u_{p,crit} = \frac{\left(\frac{2\Gamma}{d_p}\right)^{5/6}}{\left(\rho_p^3 E^2\right)^{1/6}} \quad (4)$$

Several experimental investigations quantifying deposit formation in full-scale grate-fired [19,20] and suspension-fired [21–24] boilers, have been identified in literature. However, owing to the fluctuating conditions in full-scale boilers, the experimental data cannot be used to quantify the effect of operating conditions and ash chemistry on particle/deposit sticking probability, or to accurately validate deposit build-up models. Furthermore, pilot-scale and lab-scale investigations [25–35] understanding deposit formation in biomass and kraft recovery boilers exist in literature. However, most of the investigations involve combustion of a fuel prior to deposit formation, introducing uncertainties in ash chemistry and particle size. The literature lacks fundamental and comprehensive investigations quantifying the effect of different operating conditions and ash chemistry on deposit build-up at conditions relevant for biomass-fired boilers.

The present study quantifies ash deposition on steel tubes in an Entrained Flow Reactor, at conditions simulating full-scale biomass-fired boilers. Experiments were conducted using model biomass fly ash, prepared from mixtures of $K_2Si_4O_9$, KCl, K_2SO_4, CaO, SiO_2 and KOH, as well as three different boiler fly ashes: a wood fly ash, a straw fly ash, and a straw + wood cofired fly ash. The fly ashes were injected into the reactor, to form deposits on an air-cooled deposit probe. The influence of flue gas temperature, probe surface temperature, flue gas velocity, fly ash composition, fly ash flux, fly ash particle size and probe residence time was investigated. Furthermore, selected deposit samples were analyzed using a Scanning Electron Microscope.

2 EXPERIMENTAL SECTION

2.1 Materials

Simulating the composition of typical biomass fly ash, experiments were carried out with model fly ash, prepared using mixtures of $K_2Si_4O_9$ (Alfa Aesar, CAS number: 1312-76-1), KCl (Sigma Aldrich, CAS number: 7447-40-7), K_2SO_4 (Sigma Aldrich, CAS number: 7778-80-5), CaO (Sigma Aldrich, CAS number: 1305-78-8), SiO_2 (Sigma Aldrich, CAS number: 60676-86-0) and KOH (Sigma Aldrich, CAS number: 1310-58-3). Furthermore, experiments were carried out using straw fly ash from a grate-fired boiler (Avedøreværket unit 2, 100 MW_{th}), a wood fly ash from a suspension-fired boiler (Avedøreværket unit 2, 800 MW_{th}), and a straw + wood cofired fly ash from a suspension-fired boiler (Amagerværket unit 1, 350 MW_{th}, straw share in feed ≈ 10%). The fly ashes were obtained from the electrostatic precipitator or bag filter of the boilers. The fly ash properties are provided in Table I. The median particle sizes were measured using a wet dispersion in a Malvern Mastersizer 3000. The straw fly ash was dominated by agglomerated KCl and K_2SO_4, whereas the main elements in the straw + wood cofired fly ash were Ca, Si and K. Compared to the straw + wood cofired fly ash, the wood fly ash had a lower content of K and a higher content of Si.

Table I: Composition, particle size and melting point analysis of the investigated fly ashes.

Elemental composition (wt %, dry basis)	straw fly ash, grate-fired	straw + wood cofired fly ash, suspension-fired	wood fly ash, suspension-fired
Al	–	2	2.13
Ca	1.3	20	20.8
Cl	19	1.3	0.2
Fe	0.044	1.4	1.73
K	43	9.1	6.26
Mg	0.12	3.3	3.22
Na	0.9	0.9	0.43
P	–	1.4	1.09
S	7.9	1.5	1.08
Si	1.1	12	17.7
Ti	–	0.14	–
Mn	0.059	–	–
Deformation temperature [36] (°C)	640	1240	1220
Hemispherical temperature [36] (°C)	640	1250	1230
Fluid temperature [36] (°C)	760	1260	1240
Median particle size (µm)	51.7	44.5	34.7

$K_2Si_4O_9$ particle size measurements were performed using a Malvern Mastersizer 3000, and the measurements were performed on wet and dry dispersions of the particles. Wet measurements, where the particles are dispersed in water, break down agglomerates, resulting in true particle size measurements. However, dry measurements retain particle agglomerates, revealing cluster diameters. The particle size distribution of $K_2Si_4O_9$ is provided in Figure 1. The volume-median particle diameter (D_{50}) of the wet dispersion was 13.2 µm (D_{10} = 3.47 µm, D_{90} = 29.7 µm), whereas the volume-median

particle diameter (D_{50}) of the dry dispersion was 62.3 µm (D_{10} = 7.31 µm, D_{90} = 272 µm). KCl, K_2SO_4, CaO, SiO_2 and KOH were milled and sieved individually to obtain particle sizes lower than 32 µm. The sieving process was subjected to rigorous shaking, in the presence of magnetic balls for negating static charges, and thereby breaking down agglomerates. However, it should be noted that fly ash in boilers typically forms a bimodal particle size distribution, containing submicron particles, as well as larger particles with sizes up to 200 µm [11,37].

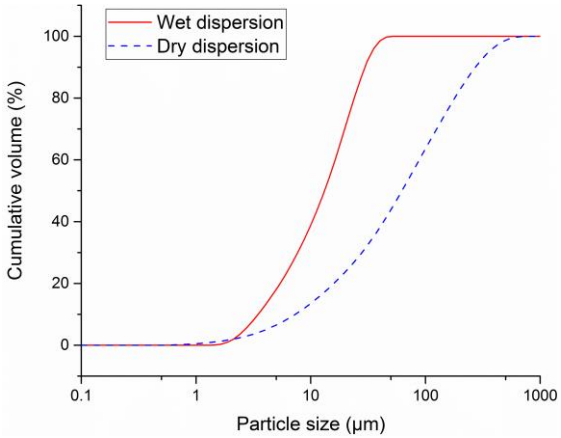

Figure 1: Particle size distribution of the investigated $K_2Si_4O_9$, obtained using Malvern Mastersizer 3000. Wet dispersion: D_{10} = 3.47 µm, D_{50} = 13.2 µm, D_{90} = 29.7 µm. Dry dispersion: D_{10} = 7.31 µm, D_{50} = 62.3 µm, D_{90} = 272 µm.

$K_2Si_4O_9$ was subjected to Differential Scanning Calorimetry (DSC), revealing that $K_2Si_4O_9$ forms a glass phase at 650 °C, after which the viscosity of $K_2Si_4O_9$ decreases with increasing temperature [38]. Additionally, Optical Dilatometry was carried out on cylindrical $K_2Si_4O_9$ pellets. The variation of normalized projected area and height of the pellet with temperature is provided in Figure 2. The ash melting analysis of $K_2Si_4O_9$, quantifying the shrinkage starting temperature, maximum shrinkage temperature, deformation temperature, hemispherical temperature and flow temperature [36] is provided in Table II.

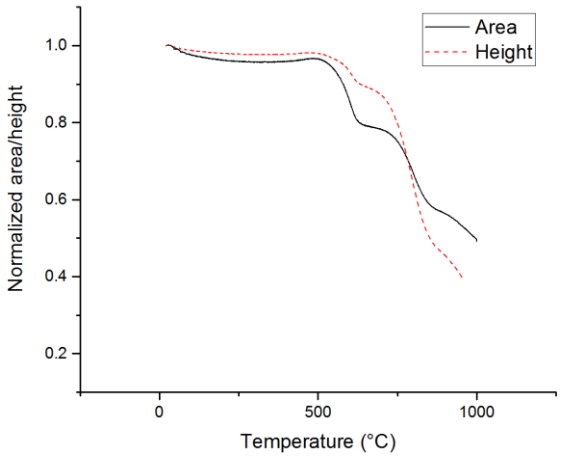

Figure 2: Optical Dilatometry of $K_2Si_4O_9$. Variation of normalized projected area and height with temperature.

Table II: Ash melting analysis of $K_2Si_4O_9$ [36], obtained using Optical Dilatometry.

Ash melting analysis	Temperature (°C)
Shrinkage starting temperature	520
Maximum shrinkage temperature	633
Deformation temperature	710
Hemispherical temperature	852
Flow temperature	1142

XRD analysis was performed on $K_2Si_4O_9$, revealing that the investigated $K_2Si_4O_9$ was completely amorphous. The majority of biomass fly ashes and deposits contain significant quantities of amorphous materials [9,22,39], including silicates [3,40,41], characterized by their viscoelastic behavior, justifying the use of $K_2Si_4O_9$ for experimental analysis.

2.2 Experimental Setup

Simulating the deposit formation process in biomass-fired boilers, experiments were carried out in an Entrained Flow Reactor (EFR). The setup consisted of a gas supply system, a screw feeder for injecting solids, a gas preheater, a 2 m long electrically heated furnace, and a fly ash deposition system comprising of an air-cooled deposit probe. A schematic representation of the setup is shown in Figure 3. A detailed description of the EFR may be found in previously published literature [42,43].

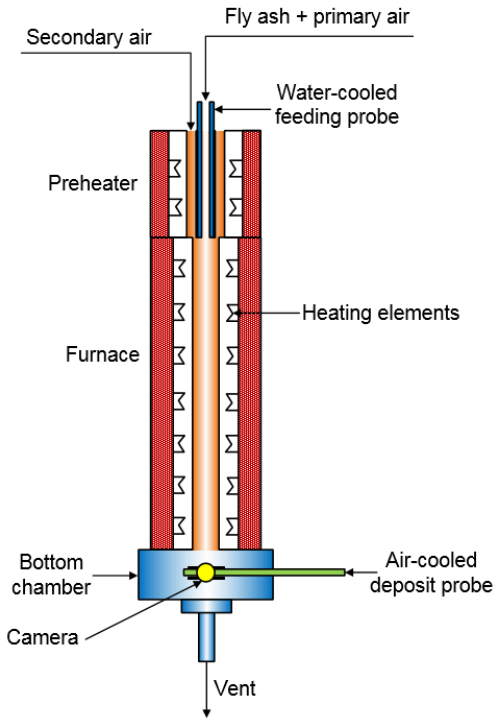

Figure 3: Schematic representation of the Entrained Flow Reactor.

The model fly ash was mixed with a primary air stream (15 NL/min), and fed into the furnace using the screw feeder. Subsequently, the inlet stream was mixed with preheated secondary air, with a maximum flow rate of 200 NL/min. The secondary air could be preheated up to 1100 °C, while the walls of the furnace could be heated up to

1450 °C. Furthermore, a purge air stream (5 NL/min) was injected into the furnace through the heating element chambers, in order to protect the heating elements from corrosion.

The model fly ash may undergo physical and chemical transformations in the furnace. It should be noted that the particle and gas temperatures in the furnace might be slightly lower than the temperature of the furnace walls. Furthermore, it was assumed that the particles in the furnace were perfectly entrained in the gas flow, resulting in equal particle and gas velocities. The terminal velocity of the $K_2Si_4O_9$ particles was estimated to be 2% of the gas velocity, using the Wen and Yu drag model [44,45], justifying the aforementioned assumption.

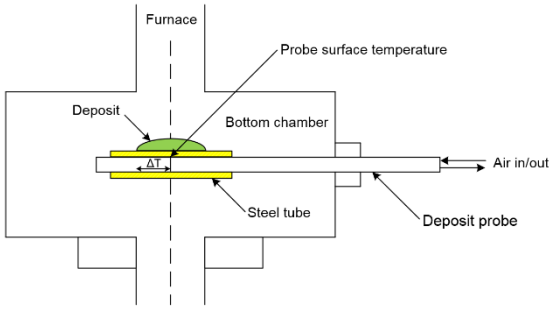

Figure 4: Air-cooled deposit probe. Deposits are formed on the steel tube mounted on the probe.

After the furnace, the entrained flow entered a bottom chamber, where the model fly ash formed deposits on a steel tube (type 316), simulating deposit formation on the first row of platen superheater tubes in boilers. Type 316 steel is commonly used in heat transfer surfaces in boilers, with its high Cr and Ni content providing superior corrosion resistance [46–48]. For each experiment, the steel deposit tubes were used as received, without any pre-oxidization. The steel tube, with an outer diameter of 10 mm, a thickness of 1 mm, and a length of 140 mm, was mounted on a retractable annular cooled probe (diameter of 8 mm), as shown in Figure 4. The probe was cooled using air preheated to 200 °C. Thermocouples were mounted on the outer surface of the deposit probe (and thereby, in contact with the inner surface of the steel tube), and the temperature at the axial centerline of the reactor (referred to as probe surface temperature, see Figure 4) was controlled electronically. The cooling probe surface temperature is analogous to steam temperature in boilers. It should be noted that the temperature at the external surface of the steel tube would be slightly higher than the cooling probe surface temperature. The difference between steel surface temperature and steam temperature in full-scale boilers is approximately 20 – 50 °C [40,49].

It should be noted that a horizontal temperature gradient was present across the deposit probe. The temperature on the deposit probe 40 mm away from either side of the axial centerline of the reactor (ΔT, see Figure 4) was typically 50 °C lower than the (central) probe surface temperature.

The bottom chamber of the EFR was water-cooled, resulting in a decrease in the flue gas temperature. Therefore, the flue gas temperature in the bottom chamber was measured by replacing the deposit probe with a suction pyrometer. It should be noted that the fly ash particles might not cool down as rapidly as the flue gas, possibly resulting in higher particle temperatures, when compared to the measured flue gas temperature in the bottom chamber.

The fly ash deposition process was recorded by a high-speed camera, mounted on a port in the bottom chamber (see Figure 3). After deposit formation for a specified duration, the deposit probe was retracted out, and the deposit was removed and weighed.

2.3 Experimental Conditions

Baseline experiments were performed at a furnace temperature of 1100 °C, resulting a flue gas temperature of 781 °C, a probe surface temperature of 475 °C, a flue gas velocity of 1 m/s, a fly ash feeding rate of 100 g/h, corresponding to a fly ash concentration of 26.57 g/Nm^3 and an ash flux of 20412 g/m^{2}h, using pure $K_2Si_4O_9$ for 15 min. In other experiments, the flue gas temperature was varied from 589 to 968 °C, the probe surface temperature was varied from 300 to 550 °C, the flue gas velocity was varied from 0.7 to 3.5 m/s, and the fly ash flux was varied from 10000 to 40000 g/m^{2}h. Fly ash particles with sizes from 3.5 to 90 µm were investigated up to a deposition time of 60 min.

Typical superheater steam temperatures in biomass-fired boilers range from 440 – 580 °C, while the flue gas temperatures in the superheater/tube bank region range from 580 – 1300 °C [21,39,49,50]. The velocity of flue gas in full-scale boilers ranges from 4 – 8 m/s [11,21]. However, since the diameter of the steel tube (10 mm) in the experiments was smaller than the typical diameter of superheater tubes in full-scale boilers (around 40 mm), lower gas velocities were adopted during the experiments in order to maintain a similar degree of Stokes number. The typical fly ash flux in biomass boilers varies from 10000 to 60000 g/m^{2}h [39], with the higher values observed during coal ash addition. In order to order to maintain a similar degree of fly ash flux in the experimental setup, higher fly ash concentrations were adopted in the experiments (13 – 53 g/Nm^3), compared to typical fly ash concentrations in full-scale biomass-fired boilers (1 – 6 g/Nm^3).

3 DEPOSIT FORMATION MODEL

A mechanistic deposit formation model was developed to simulate deposit formation of $K_2Si_4O_9$ in the reactor. The model incorporated deposit formation by thermophoresis and inertial impaction of $K_2Si_4O_9$ particles, while deposit formation by condensation was neglected due to the absence of vapor species in the gas phase.

$$\frac{dm(t,\theta)}{dt} = \dot{T}(t,\theta) + \dot{I}(t,\theta) \quad (5)$$

where m is the mass of the deposit (kg), t is the time (sec), and θ is the angular position (radians).

The rate of deposit formation by thermophoresis $\left(\dot{T}(t,\theta)\right)$ was described using Equation 6 [51].

$$\dot{T}(t,\theta) = u_T(\theta) \cdot C \cdot s(\theta) \quad (6)$$

where u_T is the thermophoretic velocity (m/s), dependent on the particle size, Knudsen's number, temperature gradient, and gas/particle thermal conductivities, C is the concentration of $K_2Si_4O_9$ (kg/m^3),

and s is the surface area of the deposit (m^2).

The rate of deposit formation by inertial impaction $\dot{I}(t,\theta)$ was described using Equation 7 [52].

$$\dot{I} = u_g \cdot C \cdot \eta_I(\theta) \cdot \eta_s(\theta) \cdot s(\theta) \quad (7)$$

where u_g is the gas velocity (m/s), η_I is the local collision efficiency of each particle, and η_s is the sticking probability of the ash particles. Since the $K_2Si_4O_9$ particles are viscoelastic in nature, the sticking probability of ash particles was estimated by accounting for energy dissipation due to particle deformation. The critical velocity of the incoming particles ($u_{p,crit}$) was calculated [53], such that

$$\eta_s = \begin{cases} 0 & u_p \cdot \sin(\alpha_{impact}) > u_{p,crit} \\ 1 & u_p \cdot \sin(\alpha_{impact}) \le u_{p,crit} \end{cases} \quad (8)$$

where u_p is the particle velocity (m/s) and α_{impact} is the angle of impaction (radians).

The critical velocity of the incoming particle is a function of the particle diameter d_p, particle density ρ_p, interface energy (surface tension) Γ and equivalent Young's modulus E [54].

$$u_{p,crit} = \frac{\left(\frac{2\Gamma}{d_p}\right)^{5/6}}{\left(\rho_p^3 E^2\right)^{1/6}} \quad (9)$$

$$\frac{1}{E} = \frac{1-\upsilon_{particle}^2}{E_{particle}} + \frac{1-\upsilon_{deposit}^2}{E_{deposit}} \quad (10)$$

where υ is the Poisson's ratio. The Young's modulus was estimated as $E = A \cdot \exp(-BT)$, where $A = 5 \cdot 10^{13}$ and $B = 0.01208$ are empirical constants obtained from literature [55].

Furthermore, the model incorporated heat transfer across the deposit layer and the steel tube, as described by Equation 11.

$$\frac{k_{tube}}{\delta_{tube}}\left(T_{tube} - T_{probe}\right) = \frac{k_{deposit}}{\delta_{deposit}}\left(T_{deposit} - T_{tube}\right) = h_{gd}\left(T_{gas} - T_{deposit}\right) + \varepsilon\sigma\left(T_{gas}^4 - T_{deposit}^4\right) \quad (11)$$

T_{gas} is the gas temperature, whereas $T_{deposit}$, T_{tube}, and T_{probe} are the temperatures at the surface of the deposit, steel tube and probe (K). k, δ, h, ε, and σ refer to the thermal conductivity (W/mK), thickness (m), heat transfer coefficient (W/m^2K), emissivity, and Stefan Boltzmann constant (W/m^2K).

The particles were assumed to be isothermal, with the corresponding heat transfer equation described in Equation 12.

$$\rho_p\left(\frac{\pi}{6}d_p^3\right)C_p\frac{dT_{particle}}{dt} = h_{gp}\left(\pi d_p^2\right)\left(T_{gas} - T_{particle}\right) + \varepsilon\sigma\left(\pi d_p^2\right)\left(T_{gas}^4 - T_{particle}^4\right) \quad (12)$$

ρ_p, C_p, d_p, and $T_{particle}$ refer to the particle density (kg/m^3), specific heat capacity (J/kgK), diameter (m), and temperature (K).

The particle size distribution measured from the dry dispersion of $K_2Si_4O_9$ particles (see Figure 1) was used in the model, to account to particle agglomeration. Model simulations have been performed only for $K_2Si_4O_9$.

Further details on the model, and equations used for estimating physical properties, can be found in previously published literature [9,53,56].

4 RESULTS AND DISCUSSION

4.1 Effect of Flue Gas Temperature

The effect of flue gas temperature on $K_2Si_4O_9$ deposit formation rate is shown in Figure 5. It was observed that the deposit formation rate increased with increasing flue gas temperature at the investigated conditions. Visual observations of the formed deposits (see Figure 5) revealed that deposits were formed only on the upstream side of the steel tube, suggesting that $K_2Si_4O_9$ deposition occurred primarily via inertial impaction, under the investigated conditions. Studies on deposit formation in full-scale boilers have also identified inertial impaction as the primary mechanism of deposit formation [11,18,40]. Increasing the flue gas temperature decreased the viscosity/Young's modulus of the $K_2Si_4O_9$ particles, thereby resulting in stickier particles, and increasing deposit formation via inertial impaction. The results were reproducible with a relative standard error of 4%, based on 5 repetitions of the baseline experiments.

The experimental results agree with full-scale investigations [21], where increasing flue gas temperatures led to increased deposit formation. Furthermore, it was observed that increasing the flue gas temperature in the experiments resulted in increased adhesion strength of the deposits to the steel tube [38].

The deposit formation model was able to predict the influence of flue gas temperature on the observed deposit formation rates with an accuracy (R^2) of 94% (see Figure 5), suggesting a fairly accurate representation of the sticking probability of the fly ash particles.

4.2 Effect of Probe Surface Temperature

Figure 5 shows the effect of probe surface temperature on the deposit formation rate. It was observed that increasing the probe surface temperature from 300 °C to 450 °C increased the deposit formation rate at the investigated conditions. Further increase in probe surface temperature up to 550 °C did not influence the rate of deposit formation significantly.

Increasing the probe surface temperature led to increased temperatures at the surface of the deposit, thereby decreasing the corresponding viscosity/Young's modulus. This resulted in an increased sticking probability of the deposit surface, causing increased deposit formation. However, it appears that increasing the probe surface temperature from 450 – 550 °C did not influence the sticking probability of the deposit surface at the investigated experimental conditions. Quantification of the temperature at the surface of the deposit is essential for understanding of the effect of probe surface temperature on the rate of deposit formation.

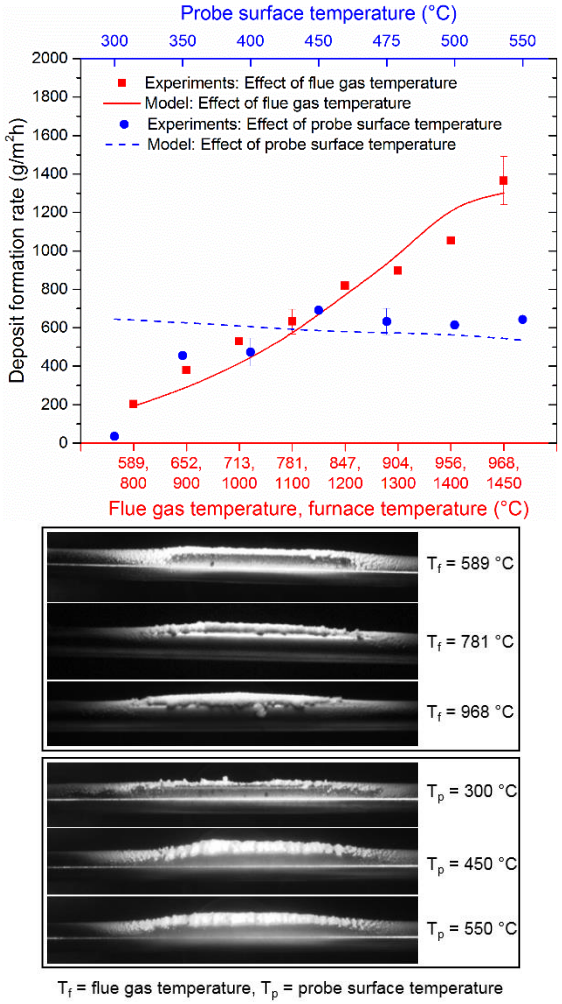

Figure 5: Effect of flue gas temperature and probe surface temperature on the deposit formation rate. Experiments performed with $K_2Si_4O_9$ with a median particle size of 13.2 µm, flue gas velocity of 1 m/s, fly ash flux of 20412 g/m^{2}h for 15 min. Flue gas temperature at the deposit probe during variation of probe surface temperature = 781 °C. Probe surface temperature during variation of flue gas temperature = 475 °C. Images captured at the end of the experiments.

The results suggest that increasing steam temperatures in boilers might increase deposit formation. However, after a certain steam temperature, determined by the thermal properties of the deposits, a further increase in the steam temperatures might not influence the rate of deposit formation. The results concur with a previous investigation in literature [27], where varying probe surface temperatures from 475 – 650 °C had a negligible effect on deposition rate of peat and straw. Nevertheless, it should be noted that high steam temperatures might lead to severe corrosion of the superheater tubes in boilers [47,49].

The model was unable to accurately predict the influence of probe surface temperature (see Figure 5), especially from 300 – 400 °C, suggesting that the sticking probability of the deposit surface requires a more accurate representation in the model. Furthermore, the deviations may have emanated from the heat transfer equations in the model, which do not account for the decrease in local gas temperatures induced by the cooling probe, especially when the probe surface temperature is maintained at 300 °C. CFD simulations of the deposit formation process in the EFR may provide more accurate model predictions. The model predicts a decrease in the deposit formation rate with increasing probe surface temperature, due to a decrease in the estimated thermophoretic deposition with reducing temperature gradients in the thermal boundary layer.

4.3 Effect of Flue Gas Velocity

Figure 6 shows the effect of flue gas velocity on the deposit formation rate for flue gas temperatures of 781 and 968 °C. At a flue gas temperature of 781 °C, it was observed that increasing the flue gas velocity from 0.7 – 3 m/s gradually decreased the deposit formation rate, with a relatively sharp decrease observed between 1 – 1.6 m/s. However, at a flue gas temperature of 968 °C, the deposit formation rate remained relatively constant from 1 – 3 m/s, and decreased in value from 3 – 3.5 m/s. Furthermore, it was observed that the thickness of the formed deposits decreased with increasing mean flue gas velocity (see Figure 6). At a mean gas velocity of 3.5 m/s and a flue gas temperature of 968 °C, it was observed that the parabolic flow profile of the flue gas was seemingly projected on the deposit surface. The flow in the furnace was laminar in nature, with Reynolds numbers ranging from 435 to 1863 under the investigated conditions. However, the Reynolds number in the bottom chamber may be larger, because of the corresponding expansion geometry.

Increasing the flue gas velocity, and thereby the particle velocity, increases the kinetic energy of the impacting particles. If the particle velocity exceeds the critical velocity of impaction, the particle is unable to dissipate its kinetic energy, and rebounds from the deposit after impaction.

The critical velocity is a function of particle size and temperature-dependent particle properties. The experimental observations suggest that the critical velocity of the $K_2Si_4O_9$ particles at a flue gas temperature of 968 °C was greater than the critical velocity at 781 °C, indicating that the critical velocity increased with increasing temperature at the investigated conditions. Since the Young's modulus is a function of viscosity, decreasing in value with increasing temperature [57,58], the critical velocity should typically increase with increasing temperature.

The model predicted a gradual decrease in the deposit formation rate with increasing flue gas velocity (see Figure 6), with an accuracy (R^2) of 38%. However, the model was unable to predict the sharp decrease in deposit formation rate at 1 m/s and 781 °C, and at 3 m/s and 968°C, probably because the model assumed a uniform plug flow in the furnace. Furthermore, agglomeration of particles in the furnace/screw feeder have not been accounted for in the model.

For particle diameters from 10 – 100 µm, at baseline conditions, the model predicted critical velocity varied from 1.4 – 0.23 m/s. These values agree with previous experimental investigations (1.2 – 0.1 m/s) in literature [15,59–62].

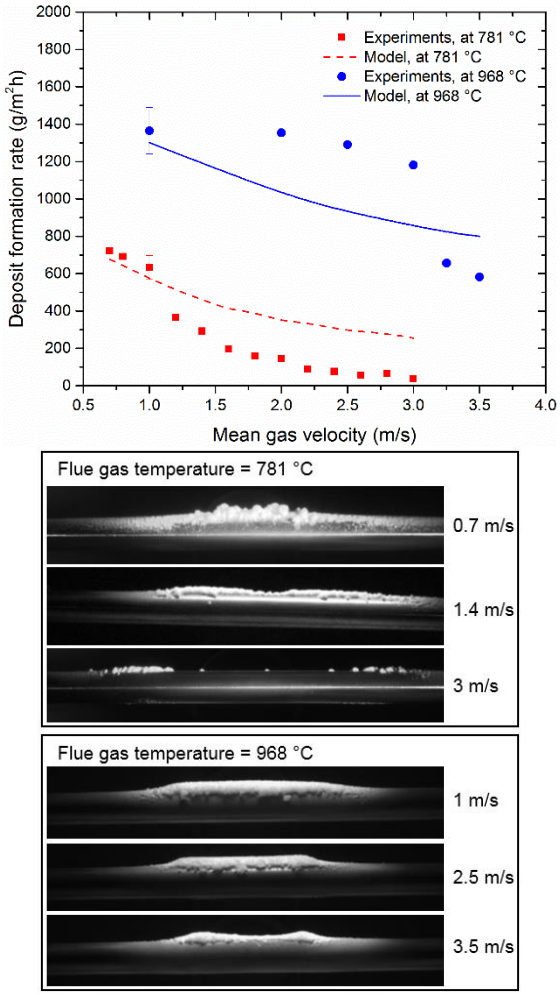

Figure 6: Effect of flue gas velocity on the deposit formation rate. Experiments performed with $K_2Si_4O_9$ with a median particle size of 13.2 µm, probe surface temperature of 475 °C, fly ash flux of 20412 g/m^{2}h for 15 min. Images captured at the end of the experiments.

4.4 Effect of Probe Residence Time

The effect of probe residence time on deposit formation rate can be seen in Figure 7. The deposit formation rate increased with time up to 30 min, at the investigated conditions. However, further increase in time did not significantly influence the deposit formation rate.

As the deposit grew in size, the temperature at the surface of the deposit increased. This resulted in a corresponding decrease in the viscosity/Young's modulus at the surface of the deposit, thereby increasing the sticking probability of the deposit surface. Therefore, the fraction of impacting particles undergoing deposition increased over time. However, the growth rate of the deposit remained constant after 30 min of deposition. Further investigation, quantifying the temperature history of the deposit surface, is required to better understand the deposit formation process. Nevertheless, the results highlight the importance of a sticky surface for deposit build-up via inertial impaction, suggesting that the rate of deposit formation on superheater tubes progressively increases as initial deposits are formed. The results are consistent with the experiments in Section 4.2, suggesting that the deposit formation rate may not further increase above a certain temperature at the surface of the deposit.

The model predicted a relatively linear increase in the deposit formation rate with time (see Figure 7), with an accuracy (R^2) of 39%. However, the model is not able to predict the saturation in deposit formation rate after 30 min, probably due to an inaccurate representation of the sticking probability of the deposit surface and/or the heat transfer model.

Due to high temperatures at the deposit surface, sintered deposits could be observed for experiments performed longer than 30 min. Furthermore, natural shedding events were observed when experiments longer than 60 min were conducted. The large deposits were unstable, breaking away from the steel tube at the deposit–tube interface. A video of deposit formation and shedding on the steel tube at the baseline conditions can be accessed via this link: youtu.be/gLSHd8fAZo0 The results concur with previous investigations [24,38], establishing debonding as the dominant mechanism of deposit shedding in boilers.

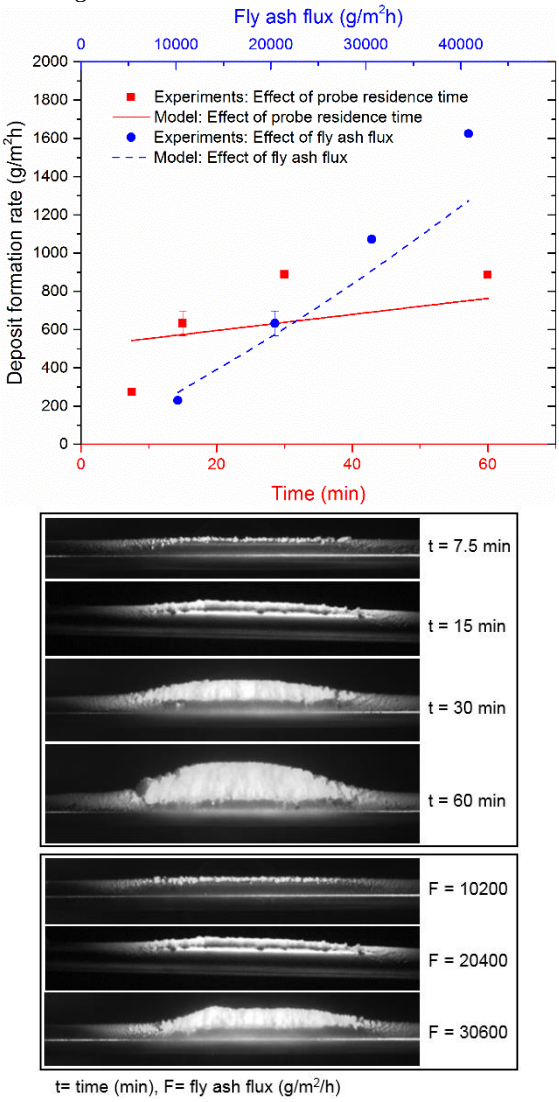

Figure 7: Effect of time and fly ash flux on the deposit formation rate. Experiments performed with $K_2Si_4O_9$ with a median particle size of 13.2 µm, flue gas temperature of 781 °C, probe surface temperature of 475 °C, and gas velocity of 1 m/s. Fly ash flux during variation of time = 20412 g/m^{2}h. Time during variation of fly ash flux = 15 min. Images captured at the end of the experiments.

4.5 Effect of Fly Ash Flux

The effect of fly ash flux on deposit formation rate can be seen in Figure 7. The deposit formation rate increased linearly with increasing fly ash flux at the investigated conditions. Increasing fly ash flux increased the total number of particles impacting the steel tube, thereby resulting in a corresponding increase in the deposit formation rate. The results agree with deposit formation models in literature [9,11], as well as full-scale investigations [19], which predict a linear increase in the rate of deposit formation via inertial impaction with increasing ash flux.

The model was able to predict the increase in deposit formation rate with increasing ash flux, with an accuracy (R^2) of 86%.

4.6 Effect of Fly Ash Particle Size

In order to understand the effect of fly ash particle size, experiments were conducted with $K_2Si_4O_9$ with a volume-median particle diameter (D_{50}) of 13.2 µm (D_{10} = 3.47 µm, D_{90} = 29.7 µm, wet dispersion, particle size distribution in Figure 1), and compared with $K_2Si_4O_9$ with a particle size distribution bounded by 32 and 90 µm. The larger particles were obtained by heating $K_2Si_4O_9$ to 800 °C to form a glass phase, which was subsequently cooled down, milled and sieved, to obtain particle sizes between 32 and 90 µm.

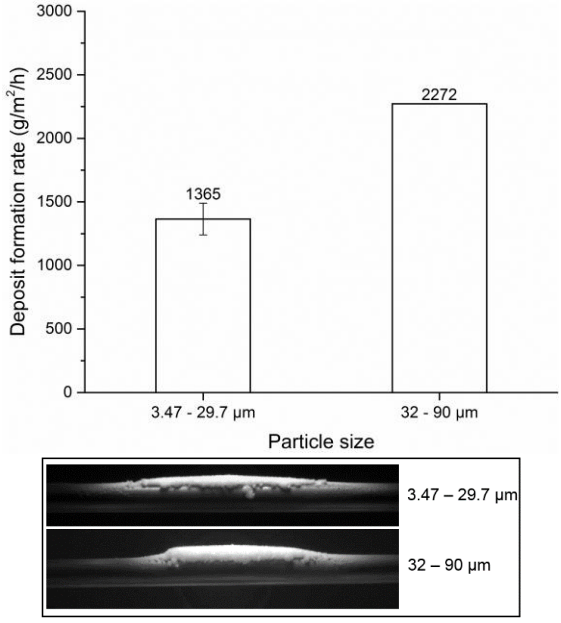

Figure 8: Effect of fly ash particle size on the deposit formation rate. Experiments performed with $K_2Si_4O_9$ with a flue gas temperature of 968 °C, probe surface temperature of 475 °C, gas velocity of 1 m/s, fly ash flux of 20412 g/m^{2}h for 15 min. Images captured at the end of the experiments.

It was observed that increasing the particle size caused increased deposit formation at the investigated conditions, as seen in Figure 8. Increasing the particle size resulted in an increase in the Stokes number, as a result of which more ash particles impacted the steel tube. Larger particles are less likely to follow the gas streamlines around the steel tube, detaching from the flow, and thereby impacting the deposit surface. This effectively increased the total mass of impacting particles, thereby increasing the rate of deposit formation.

It should be noted that increasing the particle size induced a reduction in the total number of particles injected into the furnace per unit time, since the ash flux was maintained at 20412 g/m^{2}h for the experiments. Furthermore, the effect of submicron particles in the fly ash has not been investigated in this study.

Possible agglomeration of particles in the screw feeder and the furnace was not accounted for in this study. As shown in Figure 1, agglomeration may significantly increase the effective particle size. Furthermore, the particle size measurement techniques for the smaller (3.4 – 29.7 µm) and larger (32 – 90 µm) particle size groups were different (Malvern Mastersizer vs sieves). The particle size distribution of the larger particle size group was not measured using the Malvern Mastersizer. Therefore, model predictions for the larger particle size group could not be obtained. Further investigation is required to completely understand the effect of particle size on deposit formation.

4.7 Effect of Fly Ash Composition

Model fly ash from pure compounds

The effect of fly ash composition on deposit formation is shown in Figure 9. It was observed that fly ash containing pure KCl had a greater rate of deposit formation, compared to $K_2Si_4O_9$ at the investigated conditions. Visual observations of the KCl deposit (see Figure 9) revealed deposition on both the upstream and the downstream side of the steel tube, suggesting that deposit formation had occurred by inertial impaction, as well as by condensation/thermophoresis/eddy diffusion. This is contrary to the deposits formed using $K_2Si_4O_9$, where no deposition on the downstream side was observed.

Experiments performed using CaO resulted in a low rate of deposit formation, with deposits formed only on the upstream side of the steel tube. The low rate of deposit formation can probably be attributed to the relatively high melting point of CaO (2572 °C), resulting in non-sticky particles at the investigated conditions.

However, experiments performed with SiO_2 resulted in a similar rate of deposit formation as $K_2Si_4O_9$, which is rather surprising, since SiO_2 existed in solid phase throughout the experiments, with a melting point of 1710 °C. Deposits were formed only on the upstream side of the steel tube via inertial impaction. Furthermore, XRD analysis of the deposit did not suggest any phase change or contamination. The relatively higher deposit formation rate of SiO_2 may possibly due to differences in Young's modulus, surface tension, particle hardness, etc.

Experiments using KOH revealed a high rate of deposit formation. Observations made using the camera indicated the formation of a molten film on the steel tube. At 475 °C, KOH may react with atmospheric air and form K_2CO_3. XRD analysis of the obtained deposit indicated the presence of $K_2CO_3 \cdot 1.5H_2O$ in the deposit. Deposit formation may have occurred due to impaction of KOH/K_2CO_3 droplets. Furthermore, as the flue gas cooled down from 1450 °C to 968 °C in the bottom chamber, aerosols may have been formed, which possibly underwent thermophoretic deposition on the steel tube. Moreover, KOH vapors might have heterogeneously condensed on the deposit surface.

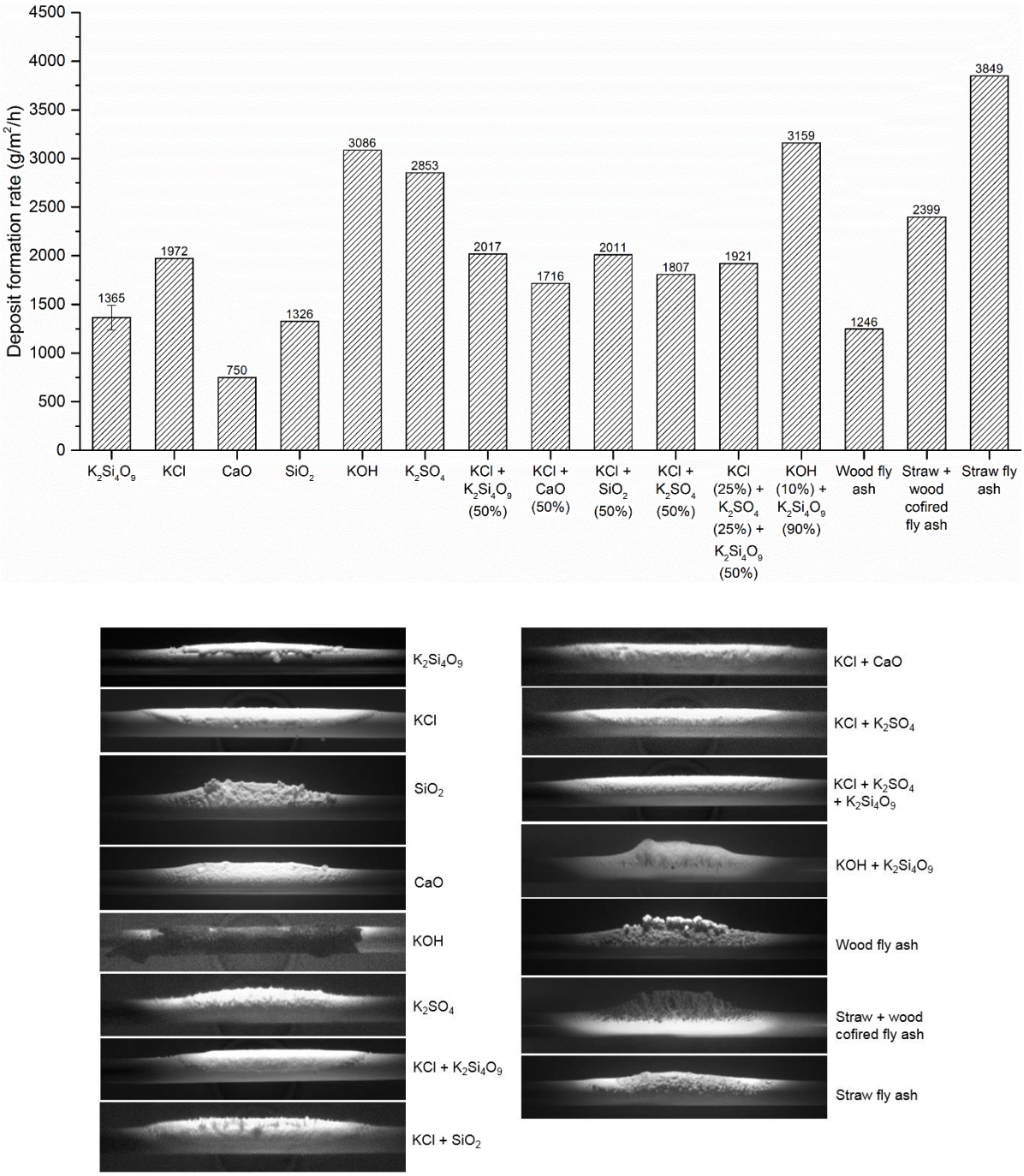

Figure 9: Effect of fly ash composition on the deposit formation rate. Experiments performed with a furnace temperature of 1450 °C, a flue gas temperature of 968 °C, probe surface temperature of 475 °C, gas velocity of 1 m/s, fly ash flux of 20412 g/m^{2}h for 15 min. $K_2Si_4O_9$ has a median particle size of 13.2 µm, whereas all other compounds have particle sizes lower than 32 µm. All compositions in wt %. Images captured at the end of the experiments.

Table III: Deposit formation rates of model fly ash mixtures. Weighted average deposit formation rate calculated from the deposit formation rate of pure compounds constituting the model fly ash mixture. Furnace temperature = 1450 °C, flue gas temperature in the bottom chamber = 968 °C, probe surface temperature = 475 °C. All compositions in wt %.

Model fly ash mixture	Experimental deposit formation rate (g/m^2h)	Weighted average deposit formation rate (g/m^2h)
$K_2Si_4O_9$	1365	
KCl	1972	
CaO	750	
SiO_2	1326	
KOH	3086	
K_2SO_4	2853	
KCl + $K_2Si_4O_9$ (50%)	2017	1669
KCl + CaO (50%)	1716	1361
KCl + SiO_2 (50%)	2011	1649
KCl + K_2SO_4 (50%)	1807	2412
KCl (25%) + K_2SO_4 (25%) + $K_2Si_4O_9$ (50%)	1921	1889
KOH (10%) + $K_2Si_4O_9$ (90%)	3159	1537
Wood fly ash	1246	1223
Straw + wood cofired fly ash	2399	1296
Straw fly ash	3849	2364

Experiments using K_2SO_4 resulted in a high deposit formation rate (2853 g/m^2h), relative to the deposit formation rate of KCl and $K_2Si_4O_9$. Furthermore, deposition was observed on both sides of the steel tube, indicating deposition by inertial impaction as well as condensation/thermophoresis.

The results obtained from the aforementioned deposits concur with full-scale studies in straw-fired boilers [19], where increasing concentration of K and S in the fuel resulted in an increase in the formation of hard deposits.

Model fly ash from mixtures of compounds

Experiments conducted with a model fly ash generated from a mixture of KCl and $K_2Si_4O_9$ (50 wt %) revealed that the mixture of KCl and $K_2Si_4O_9$ had a higher rate of deposit formation, when compared to the weighted average deposit formation rate of pure KCl and pure $K_2Si_4O_9$ (see Table III). This indicates that the addition of KCl influenced the sticking probability of $K_2Si_4O_9$ particles and/or the deposit surface.

A condensation layer was observed on the downstream side, whereas a thick layer, formed primarily via inertial impaction, was observed on the upstream side of the steel tube. The thick layer was removed and analyzed using a Scanning Electron Microscope, revealing the following observations,

- As shown in Figure 10a, tiny KCl particles, approximately 5 µm in diameter, were observed on the surface of the $K_2Si_4O_9$ particles. In the bottom chamber, KCl may have existed as vapors, aerosols or molten droplets at the investigated conditions. The observed phenomenon is probably heterogeneous condensation of KCl vapors on $K_2Si_4O_9$ particles, or agglomeration/scavenging of KCl aerosols or tiny molten droplets on $K_2Si_4O_9$ particles. This may have occurred in-flight on $K_2Si_4O_9$ particles, prior to deposit formation, or on $K_2Si_4O_9$ particles present in the deposit. Nevertheless, a layer of partially molten KCl on the $K_2Si_4O_9$ particles decreases the surface viscosity (or increases the melt fraction) of the particles. In-flight heterogeneous condensation/scavenging of KCl on $K_2Si_4O_9$ particles may have increased the sticking probability of the $K_2Si_4O_9$ particles, whereas heterogeneous condensation/agglomeration of KCl on $K_2Si_4O_9$ particles present in the deposit may have increased the sticking probability of the deposit surface. Therefore, due to the presence of KCl on the deposit surface, and possibly on the surface of in-flight $K_2Si_4O_9$ particles, the deposit formation rate of $K_2Si_4O_9$ increased.
- A majority of the $K_2Si_4O_9$ particles in the deposit were glued together by molten KCl, as shown in Figure 10b. This may have been due to molten KCl droplets impacting the deposit surface, and subsequently spreading out to form a neck between adjacent $K_2Si_4O_9$ particles in the deposit. Furthermore, condensation of KCl vapors on the deposit surface may have induced sintering [3], forming a bridge between adjacent $K_2Si_4O_9$ particles. Investigation of deposit composition and morphology in full-scale biomass boilers has shown that the Si and Ca rich particles, found in the intermediate and outer layers of the deposit, were glued together by KCl [19,40], agreeing with the experimental observations.

Similarly, the model fly ash mixtures KCl + CaO (50 wt %) and KCl + SiO_2 (50 wt %) showed an increased deposit formation rate, when compared to their respective weighted average deposit formation rates (see Table III). Deposition was observed on both sides of the steel tube (see Figure 9).

However, the model fly ash mixture KCl + K_2SO_4 (50 wt %) showed a decreased deposit formation rate, when compared to its weighted average deposit formation rate (see Table III). Deposition was observed on both sides of the steel tube (see Figure 9). Conclusive inferences cannot be obtained currently, and the deposition behavior of K_2SO_4 requires further investigation.

The model fly ash mixture KCl (25 wt %) + K_2SO_4 (25 wt %) + $K_2Si_4O_9$ (50 wt %) showed an increased deposit formation rate, when compared to its weighted average deposit formation rate (see Table III). Deposition was observed on both sides of the steel tube (see Figure 9).

Experiments conducted with a model fly ash containing KOH (10 wt %) and $K_2Si_4O_9$ (90 wt %) indicated that addition of KOH significantly increased the deposit formation rate of $K_2Si_4O_9$ at the investigated conditions (see Table III). Visual observations of the deposit revealed that the majority of deposition occurred

on the upstream side of the steel tube via inertial impaction, with a thin condensation layer present on the downstream side of the steel tube (see Figure 9). Heterogeneous condensation/agglomeration of KOH vapors/aerosols on $K_2Si_4O_9$ particles may have occurred, increasing the sticking probability of the $K_2Si_4O_9$ particles. The presence of KOH in boiler deposits has been postulated in a few studies in literature [6,63]. The results indicate that presence of even small quantities of KOH in the boiler may exacerbate fly ash deposition on boiler surfaces.

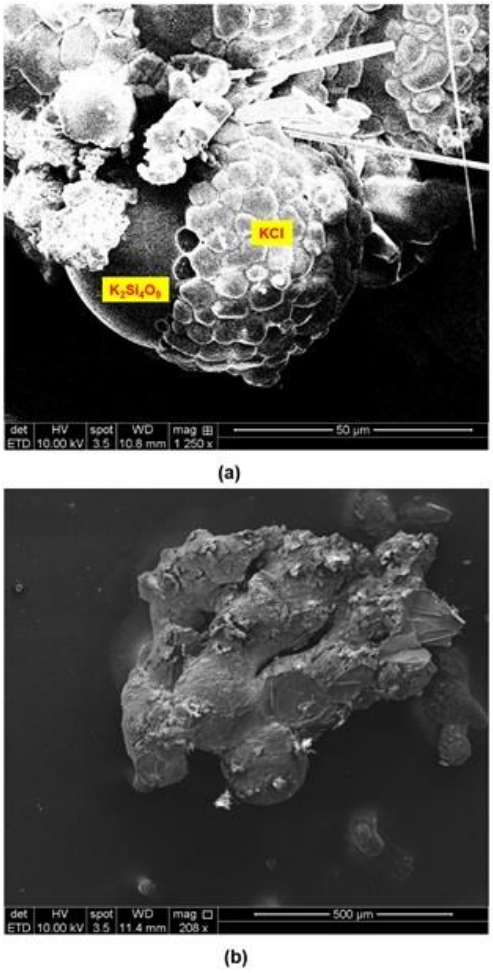

Figure 10: SEM image of deposit particles. Experiments performed with KCl + $K_2Si_4O_9$ (50 wt %) with a furnace temperature of 1450 °C, a flue gas temperature of 968 °C, probe surface temperature of 475 °C, gas velocity of 1 m/s, fly ash flux of 20412 g/m^{2}h for 15 min. $K_2Si_4O_9$ has a median particle size of 13.2 µm, whereas KCl has particle sizes lower than 32 µm. (a) Tiny KCl nuclei on $K_2Si_4O_9$ particles. (b) $K_2Si_4O_9$ particles in the deposit glued together by molten KCl.

The results from this section suggest that interaction among the constituents of the model fly ash may significantly influence its overall deposition behavior. Addition of KCl/KOH to $K_2Si_4O_9$, SiO_2, and CaO resulted in increased deposit formation rates, when compared to their respective weighted average deposit formation rates. However, the deposition behavior of K_2SO_4, and the KCl–K_2SO_4 system has not been understood completely, requiring further investigation.

Corrosion and adhesion strength of the investigated model fly ash deposits

Inspection of the deposits and the steel tube after the experiments showed that the steel tubes experienced corrosion if the model fly ash contained KCl or KOH. Furthermore, presence of KCl, K_2SO_4, $K_2Si_4O_9$ or KOH in the model ash fly mixture resulted in relatively strongly adherent deposits at the investigated conditions. However, presence of CaO or SiO_2 resulted in low adhesion strength of the formed deposits. The results agree with the previous investigations on deposit adhesion strength [38].

Fly ash obtained from biomass-fired boilers

Experiments comparing the deposit formation rates of three different boiler fly ashes (see Table I) revealed that the investigated wood fly ash exhibited the least deposit formation rate, and the investigated straw + wood cofired fly ash exhibited a moderately high deposit formation rate, whereas the deposit formation rate of the investigated straw fly ash was significantly high (see Figure 9). Visual observations of the deposits indicated that wood fly ash and the straw + wood cofired fly ash formed a thin layer on the lateral sides of the steel tube, probably from thermophoretic deposition, whereas a porous, weakly adherent deposit layer was formed on the upstream side. However, no corrosion was observed at the deposit–tube interface. The deposition adhesion strength of the straw + wood cofired fly ash was slightly greater than the wood fly ash. The deposit formation rate of the wood fly ash was similar in magnitude to the weighted average deposit formation rate of its constituents, whereas the deposit formation rate of the straw + wood cofired fly ash was greater than the corresponding weighted average deposit formation rate (see Table III).

The straw fly ash formed deposits on both sides of the steel tube, probably via condensation, thermophoresis and inertial impaction. The deposit was extremely dense and strongly adherent to the steel tube, causing corrosion at the deposit–tube interface. The deposit formation rate of the straw fly ash was greater than the weighted average deposit formation rate of its constituents (see Table III). The high deposit formation rate of straw fly ash can be attributed to the high concentration of K, Cl and S in straw fly ash. Furthermore, the relatively low deformation temperature of straw fly ash (640 °C, see Table I) indicates that the fly ash may have existed as molten droplets or vapor species, leading to a high rate of deposit formation. Moreover, the median particle size of the straw fly ash was relatively large.

The straw share in the boiler feed for generating the straw + wood cofired fly ash was approximately 10%. The high rate of deposit formation of the straw + wood cofired fly ash in the experiments, compared to the wood fly ash and the weighted average deposit formation rate, suggests that addition of relatively low shares of straw in the feed, while cofiring straw and wood, may lead to a considerable increase in deposit formation.

The experimental results agree with full-scale studies on deposit formation, where increasing straw content in the feed resulted in increased deposit formation rates [21,22,24,28]. Furthermore, full-scale studies have indicated that increasing alkali content in the fuel causes higher deposit formation rates [19,20,64].

The results show that ash chemistry has a significant influence on deposit formation rates in biomass boilers. Furthermore, physical and chemical interactions between

the components of the fly ash may increase or decrease deposit formation. However, further investigation is required to completely understand the effect of ash chemistry and ash transformations on deposit build-up in boilers.

5 CONCLUSIONS

The deposit formation of biomass fly ash on a steel tube in a laboratory-scale Entrained Flow Reactor was investigated in this study. Experiments were conducted using model biomass fly ash, prepared from mixtures of $K_2Si_4O_9$, KCl, K_2SO_4, CaO, SiO_2 and KOH, as well as three different boiler fly ashes: a wood fly ash, a straw fly ash, and a straw + wood cofired fly ash. The fly ashes were injected into the reactor, to form deposits on an air-cooled probe, simulating deposit formation on the first row of platen superheater tubes in biomass-fired boilers. The effect of flue gas temperature, probe surface temperature, flue gas velocity, fly ash composition, fly ash flux, fly ash particle size and probe residence time was investigated.

The results revealed that increasing the flue gas temperature from 589 – 968 °C increased the sticking probability of the model fly ash particles, thereby resulting in higher deposit formation rates. Furthermore, increasing the probe surface temperature from 300 – 450 °C increased the sticking probability of the deposit surface, resulting in increased deposit formation. However, varying the probe surface temperature from 450 – 550 °C did not influence the deposit formation rate at the investigated conditions. Increasing flue gas velocity from 0.7 – 3.5 m/s, and thereby the particle velocity, resulted in a decrease in the rate of deposit formation, since an increase in the kinetic energy of the particles results in increased particle rebound from the deposit surface after impaction.

The deposit formation rate increased with time, since an increasing deposit thickness led to higher temperatures at the deposit surface, thereby increasing the sticking probability of the deposit surface. However, the growth rate of the deposit was constant after 30 min at the investigated conditions. Furthermore, increasing fly ash flux resulted in a linear increase in the deposit formation rate. Increasing the particle size of the fly ash resulted in an increased rate of deposit formation, since larger particles are more likely to detach from the gas streamlines around the steel tube and impact the tube surface.

A mechanistic model was developed to predict deposit formation in the reactor. The model was able to reasonably predict the influence of flue gas temperature and fly ash flux, suggesting that accounting for energy dissipation due to particle deformation, for predicting the sticking probability of incoming ash particles, seems to be fairly successful in predicting the influence of changes in local conditions on the deposit formation process. However, the model was unable to accurately predict the influence of probe surface temperature, gas velocity and probe residence time. Improvements in the prediction of the sticking probability of the deposit surface, as well as CFD simulations of the deposit formation process in the reactor, are desirable to improve model predictions.

Inertial impaction was the primary mechanism of deposit formation, when pure $K_2Si_4O_9$, SiO_2 or CaO was injected into the reactor, forming deposits only on the upstream side of the steel tube. However, feeding KCl, K_2SO_4 or KOH into the reactor resulted in deposit formation on both sides of the steel tube, via condensation, thermophoresis, and inertial impaction. The model fly ash containing pure KOH resulted in the largest rate of deposit formation, followed by K_2SO_4, KCl, $K_2Si_4O_9$, SiO_2 and CaO.

Addition of KCl to $K_2Si_4O_9$, SiO_2, and CaO resulted in an increased deposit formation rate, when compared to their respective weighted average deposit formation rates. Addition of KCl influenced the sticking probability of the deposit surface, and possibly the sticking probability the in-flight $K_2Si_4O_9$, SiO_2, and CaO particles. Moreover, addition of KOH to $K_2Si_4O_9$ in the model fly ash mixture resulted in a significant increase in the deposit formation rate. Experiments using three different boiler fly ashes revealed a low rate of deposit formation for the investigated wood fly ash, and a high rate of deposit formation for the straw fly ash. Analysis of deposits obtained using a model fly ash containing KCl and $K_2Si_4O_9$ (50 wt %), using a Scanning Electron Microscope, revealed the presence of tiny KCl nuclei on $K_2Si_4O_9$ particles. Furthermore, the $K_2Si_4O_9$ particles in the deposit were glued together by molten KCl.

The obtained results provide an improved understanding of deposit formation in boilers, describing the influence of operating conditions and ash chemistry. Furthermore, the experimental data may be used to develop novel sticking criteria to predict deposit growth in full-scale boilers.

6 ACKNOWLEDGEMENTS

This work is part of the project, 'Flexible use of Biomass on PF fired power plants' funded by Energinet.dk through the ForskEL programme, DONG Energy and DTU.

7 REFERENCES

[1] The Danish Government. Our Future Energy. 2011. ISBN: 978-87-7844-915-3.

[2] A. Zbogar, F. Frandsen, P.A. Jensen, P. Glarborg. Prog. Energy Combust. Sci. 35 (1) (2009) pag. 31–56.

[3] F. Frandsen. Ash formation, deposition and corrosion when utilizing straw for heat and power production. Technical University of Denmark, Department of Chemical and Biochemical Engineering, 2010. ISBN: 978-87-92481-40-5.

[4] S.C. Okoro, M. Montgomery, F.J. Frandsen, K. Pantleon. Energy Fuels 28 (10) (2014) pag. 6447–6458.

[5] A.J. Damoe, P.A. Jensen, F.J. Frandsen, H. Wu, P. Glarborg. Energy and Fuels 31 (1) (2017) pag. 555–570.

[6] H. Wu, M.S. Bashir, P.A. Jensen, B. Sander, P. Glarborg. Fuel 113 (2013) pag. 632–643.

[7] K.A. Christensen, M. Stenholm, H. Livbjerg. J. Aerosol Sci. 29 (4) (1998) pag. 421–444.

[8] K.A. Christensen. The formation of submicron particles from the combustion of straw. Department of Chemical Engineering. Technical University of Denmark; 1995. ISBN: 8790142047.

[9] S.B. Hansen, P. Glarborg, F.J. Frandsen, P.A. Jensen. Model for Deposition Build-up in Biomass Boilers. Technical University of Denmark, 2015.

[10] L.L. Baxter. Biomass Bioenergy 4 (2) (1993) pag.

85–102.
[11] H. Zhou, P.A. Jensen, F.J. Frandsen. Fuel 86 (10–11) (2007) pag. 1519–1533.
[12] D.E. Rosner, P. Tandon. Chem. Eng. Sci. 50 (21) (1995) pag. 3409–3431.
[13] R.A. Wessel, J. Righi. Aerosol Sci. Technol. 9 (1) (1988) pag. 29–60.
[14] P.M. Walsh, A.N. Sayre, D.O. Loehden, L.S. Monroe, J.M. Beér, A.F. Sarofim. Prog. Energy Combust. Sci. 16 (4) (1990) pag. 327–345.
[15] M. Dong, J. Han, S. Li, H. Pu. Energies 6 (12) (2013) pag. 4288–4307.
[16] S. Chen, S. Li, M. Yang. Powder Technol. 274 (2015) pag. 431–440.
[17] K.L. Johnson, K. Kendall, A.D. Roberts. Proc. R. Soc. A Math. Phys. Eng. Sci. 324 (1558) (1971) pag. 301–313.
[18] U. Kleinhans, C. Wieland, S. Babat, G. Scheffknecht, H. Spliethoff. Proc. Combust. Inst. 36 (2) (2017) pag. 2341–2350.
[19] P.A. Jensen, M. Stenholm, P. Hald. Energy Fuels 11 (5) (1997) pag. 1048–1055.
[20] A. Žbogar, P.A. Jensen, F.J. Frandsen, J. Hansen, P. Glarborg. Energy Fuels 20 (2) (2006) pag. 512–519.
[21] M.S. Bashir, P.A. Jensen, F. Frandsen, S. Wedel, K. Dam-Johansen, J. Wadenbäck, et al. Fuel Process. Technol. 97 (2012) pag. 93–106.
[22] D. Nordgren, H. Hedman, N. Padban, D. Boström, M. Öhman. Fuel Process. Technol. 105 (2013) pag. 52–8.
[23] B.J. Skrifvars, T. Laurén, M. Hupa, R. Korbee, P. Ljung. Fuel 83 (10) (2004) pag. 1371–1379.
[24] M.S. Bashir, P.A. Jensen, F. Frandsen, S. Wedel, K. Dam-Johansen, J. Wadenbäck, et al. Energy Fuels 26 (4) (2012) pag. 2317–2330.
[25] M. Theis, B.-J. Skrifvars, M. Hupa, H. Tran. Fuel 85 (7–8) (2006) pag. 1125–1130.
[26] M. Theis, B.-J. Skrifvars, M. Zevenhoven, M. Hupa, H. Tran. Fuel 85 (14–15) (2006) pag. 1992–2001.
[27] M. Theis, B.J. Skrifvars, M. Zevenhoven, M. Hupa, H. Tran. Fuel 85 (14–15) (2006) pag. 2002–11.
[28] S.S. Lokare, J.D. Dunaway, D. Moulton, D. Rogers, D.R. Tree, L.L. Baxter. Energy Fuels 20 (3) (2006) pag. 1008–1014.
[29] G. Li, S. Li, X. Xu, Q. Huang, Q. Yao. Energy Fuels 28 (1) (2014) pag. 219–227.
[30] R. Shenassa, H. Tran, D.C.S. Kuhn. Pulp Pap. Canada 100 (10) (1999) pag. 56–62.
[31] A. Regueiro, D. Patiño, E. Granada, J. Porteiro. Appl. Therm. Eng. 112 (2017) pag. 523–533.
[32] T. Heinzel, V. Siegle, H. Spliethoff, K.R.G. Hein. Fuel Process. Technol. 54 (1998) pag. 109–125.
[33] A.L. Robinson, H. Junker, L.L. Baxter. Energy Fuels 16 (2) (2002) pag. 343–355.
[34] T. Madhiyanon, P. Sathitruangsak, S. Sungworagarn, S. Pipatmanomai, S. Tia. Fuel Process. Technol. 96 (2012) pag. 250–264.
[35] P. Teixeira, H. Lopes, I. Gulyurtlu, N. Lapa, P. Abelha. Biomass Bioenergy 39 (2012) pag. 192–203.
[36] European Committee for Standardization. Solid biofuels- Method for the determination of ash melting behaviour - Part 1: Characteristic temperatures method, CEN/TS 15370-1:2006. 2006.
[37] J. Pagels, M. Strand, J. Rissler, A. Szpila, A. Gudmundsson, M. Bohgard, et al. J. Aerosol Sci. 34 (8) (2003) pag. 1043–1059.
[38] Y. Laxminarayan, P.A. Jensen, H. Wu, F.J. Frandsen, B. Sander, P. Glarborg. Energy Fuels 31 (8) (2017) pag. 8733–8741.
[39] H. Wu, M.S. Bashir, P.A. Jensen, B. Sander, P. Glarborg. Fuel 113 (2013) pag. 632–643.
[40] P.A. Jensen, F.J. Frandsen, J. Hansen, K. Dam-Johansen, N. Henrisken, S. Hörlyck. Energy Fuels 18 (2) (2004) pag. 378–384.
[41] L.A. Hansen, H.P. Nielsen, F.J. Frandsen, K. Dam-Johansen, S. Hørlyck, A. Karlsson. Fuel Process. Technol. 64 (1) (2000) pag. 189–209.
[42] H. Wu, P. Glarborg, F.J. Frandsen, K. Dam-Johansen, P.A. Jensen. Energy Fuels 25 (7) (2011) pag. 2862–2873.
[43] Y. Zheng, P.A. Jensen, A.D. Jensen, B. Sander, H. Junker. Fuel 86 (7–8) (2007) pag. 1008–1020.
[44] C.Y. Wen, Y.H. Yu. Chem. Eng. Prog. Symp. Ser. 62 (1966) pag. 100–111.
[45] W. Yang. Ind. Eng. Chem. Fundam. 12 (3) (1973) pag. 349–352.
[46] J. Lai. Mater. Sci. Eng. 58 (1983) pag. 195–209.
[47] A. Zahs, M. Spiegel, H.J. Grabke. Corros. Sci. 42 (6) (2000) pag. 1093–1122.
[48] T. Yukitoshi, K. Yoshikawa, T. Daikoku, F. Masuyama. J. Mater. Energy Syst. 4 (2) (1982) pag. 99–109.
[49] M. Montgomery, A. Karlsson, O.H. Larsen. Mater. Corros. 53 (2) (2002) pag. 121–131.
[50] M. Montgomery, S.A. Jensen, U. Borg, O. Biede, T. Vilhelmsen. Mater. Corros. 62 (7) (2011) pag. 593–605.
[51] C. He, G. Ahmadi. Aerosol Sci. Technol. 29 (6) (1998) pag. 525–546.
[52] H. Zhou, P.A. Jensen, F.J. Frandsen. Fuel 86 (10–11) (2007) pag. 1519–1533.
[53] S.B. Hansen, P.A. Jensen, F.J. Frandsen, B. Sander, P. Glarborg. Energy Fuels 31 (3) (2017) pag. 2771–2789.
[54] C. Thornton, Z. Ning. Powder Technol. 99 (2) (1998) pag. 154–162.
[55] W. Ai, J.M. Kuhlman. Energy Fuels 25 (2) (2011) pag. 708–718.
[56] Y. Laxminarayan. Formation, Sintering and Removal of Biomass Ash Deposits. Technical University of Denmark, 2018.
[57] M. Losurdo, H. Spliethoff, J. Kiel. Fuel 102 (2012) pag. 145–155.
[58] W.D. Callister. Materials science and engineering : an introduction. John Wiley & Sons; 2007. ISBN: 0-471-73696-1.
[59] M. Dong, S. Li, J. Xie, J. Han. Energies 6 (12) (2013) pag. 3245–3262.
[60] L.N. Rogers, J. Reed. J. Phys. D. Appl. Phys. 17 (4) (1984) pag. 677–689.
[61] H.-C. Wang, W. John. Dynamic adhesion of particles impacting a cylinder. Part. Surfaces 1, Springer; 1988, pag. 211–24.
[62] N.A. Esmen, P. Ziegler, R. Whitfield. J. Aerosol Sci. 9 (6) (1978) pag. 547–556.
[63] N. Folkeson, T. Jonsson, M. Halvarsson, L.-G. Johansson, J.-E. Svensson. Mater. Corros. 62 (7) (2011) pag. 606–615.
[64] L. Tobiasen, R. Skytte, L.S. Pedersen, S.T. Pedersen, M.A. Lindberg. Fuel Process. Technol. 88 (11–12) (2007) pag. 1108–1117.